View metadata, citation and similar papers at core.ac.uk

brought to you by CORE

provided by Kyoto University Research Information Repository

KURENAI
Kyoto University Research Information Repository

KYOTO UNIVERSITY

Title	Suddenly shortened half-lives beyond ^{78}Ni : N = 50 magic number and high-energy nonunique first-forbidden transitions
Author(s)	Yoshida, Kenichi
Citation	Physical Review C (2019), 100(2)
Issue Date	2019-08
URL	http://hdl.handle.net/2433/243834
Right	© 2019 The American Physiological Society; This is the accepted version of the article, which has been published in final form at http://doi.org/10.1103/PhysRevC.100.024316.
Type	Journal Article
Textversion	publisher

Kyoto University

Suddenly shortened half-lives beyond ^{78}Ni: $N = 50$ magic number and high-energy nonunique first-forbidden transitions

Kenichi Yoshida
Department of Physics, Kyoto University, Kyoto, 606-8502, Japan

(Received 8 March 2019; revised manuscript received 1 July 2019; published 12 August 2019)

Background: β-decay rates play a decisive role in understanding the nucleosynthesis of heavy elements and are governed by microscopic nuclear-structure information. A sudden shortening of the half-lives of Ni isotopes beyond $N = 50$ was observed at the RIKEN-RIBF. This is considered due to the persistence of the neutron magic number $N = 50$ in the very neutron-rich Ni isotopes.
Purpose: By systematically studying the β-decay rates and strength distributions in the neutron-rich Ni isotopes around $N = 50$, I try to understand the microscopic mechanism for the observed sudden shortening of the half-lives.
Methods: The β-strength distributions in the neutron-rich nuclei are described in the framework of nuclear density-functional theory. I employ the Skyrme energy-density functionals (EDF) in the Hartree-Fock-Bogoliubov calculation for the ground states and in the proton-neutron quasiparticle random-phase approximation (pnQRPA) for the transitions. Not only the allowed but the first-forbidden (FF) transitions are considered.
Results: The experimentally observed sudden shortening of the half-lives beyond $N = 50$ is reproduced well by the calculations employing the Skyrme SkM* and SLy4 functionals in contrast to the monotonic shortening predicted in the preceding calculation using the SkO' functional.
Conclusions: The sudden shortening of the half-lives beyond $N = 50$ in the neutron-rich Ni isotopes is due to the shell gap at $N = 50$ and cooperatively with the high-energy transitions to the low-lying 0^- and 1^- states in the daughter nuclei. The onset of FF transitions pointed out around $N = 82$ and 126 is preserved in the lower-mass nuclei around $N = 50$. This study suggests that a microscopic calculation is needed, where the shell structure in neutron-rich nuclei and its associated effects on the FF transitions are self-consistenly taken into account for predicting β-decay rates of exotic nuclei in unknown region.

DOI: 10.1103/PhysRevC.100.024316

I. INTRODUCTION

Magic numbers are a key quantity to understand the quantum many-body systems such as atomic nuclei. This is because the single-particle motion in a mean-field potential and the associated shell structure are important concepts in nuclear structure. The local stability with the specific combinations of neutrons and protons is naturally understood with the help of the magic numbers. The canonical values were established in the systematic studies of nuclei along the β stability line. In the recent studies of neutron-rich nuclei, however, it was found that some of the magic numbers disappear and new ones show up instead [1]. Exploring the evolution of the shell structures and elucidating the underlying mechanism as functions of the neutron and proton numbers have been a fundamental research topic in the field of nuclear physics [2].

The neutron magic number $N = 50$ around the very neutron-rich nucleus ^{78}Ni ($N/Z \sim 1.8$) has attracted a considerable interest, not only in a view of nuclear structure, but in a point of the r-process nucleosynthesis: ^{78}Ni can be a doubly magic nucleus and an important waiting point serving as a bottleneck in the synthesis of heavy elements [3]. Therefore, there have been numerous numbers of experimental efforts on if the $N = 50$ magic number survives in ^{78}Ni [4–16].

Though single-particle energies in a spherical mean field are not a direct observable, two-nucleon and one-nucleon separation energies are often considered as a corresponding signature. A high-precision nuclear mass measurement at the Ion Guide Isotope Separation On-Line (IGISOL) on the $Z = 30$–33 nuclei with a mass number around 80–90 revealed a reduction of the $N = 50$ shell gap energy towards Ge ($Z = 32$) and an increase at Ga ($Z = 31$) [4], where the experimental shell-gap energy was defined by the difference of the two-neutron separation energies as $\Delta_n(N) = S_{2n}(N) - S_{2n}(N + 2)$. By comparing some mean-field calculations and mass models, Hakala *et al.* in Ref. [4] obtained an indication of the persistent $N = 50$ shell gap in ^{78}Ni. The recent measurement on ^{79}Cu at the CERN-ISOLDE revealed a reduction of the $N = 48$ shell gap, suggesting indirectly the enhanced $N = 50$ shell gap [5]. Another mass measurement on the Zn ($Z = 30$) isotopes including ^{81}Zn confirmed that the $N = 50$ shell gap is maintained for the Zn isotopes by looking at the one-neutron separation energies, and supports the indication above [6]. Porquet and Sorlin pointed out that the linear fits to the one-neutron separation energies lead to a diminished $N = 50$ shell gap energy in ^{78}Ni, where the collective effect at $Z = 32$ was carefully examined [7]. On the other hand, the

 ©2019 American Physical Society

large-scale shell-model calculation explaining these observations predicted a persistent shell closure in ^{78}Ni [17].

The low-lying quadrupole state is sensitive to the softness of a spherical nucleus against quadrupole deformation. Thus, the excitation energy of the first-excited 2^+ state and the transition matrix element are also a possible signature of the rigidity at magic numbers. A systematic investigation on the low- and medium-spin states in the $N = 50$ isotones with $Z = 32$–37 suggests a constant $N = 50$ shell gap by comparing to the shell-model calculation [8]. The lowering of transition probability $B(E2)$ in the Ge isotopes up to ^{82}Ge also indicates that the $N = 50$ shell closure remains in the neutron-rich nuclei [9–11]. The higher energy of the 2_1^+ state and the lower $B(E2)$ value measured in ^{80}Zn [12] and the recently observed 4_1^+ state [13] further confirmed the persistent $N = 50$ shell closure in ^{78}Ni. However, looking at the Ni isotopes, the $E(2_1^+)$ value decreases up to $N = 48$ and the $B(E2)$ value increases up to $N = 46$ [14]. Thus, the "direct" measurement of the $E(2_1^+)$ and $B(E2)$ in ^{78}Ni is strongly desired [15], while the recent theoretical calculations predicted the doubly closed structure in ^{78}Ni [18,19].

Even though the production yields are small and the experiments on the mass or the low-lying quadrupole state are difficult to perform, the measurement of β-decay half-lives $T_{1/2}$ is feasible. Thus, there have been some attempts to study the structure of very neutron-rich nuclei via half-lives. The β-decay $T_{1/2}$ were discussed in terms of the shell effects, in particular the nuclear deformation effect, in the S and Cl nuclei with $N = 28$ [20] and in the $N \simeq 40$ nuclei around ^{64}Cr [21]. In these works, the measured $T_{1/2}$ were compared to the results of model calculations such as the finite range droplet model+quasiparticle random-phase approximation (FRDM+QRPA) [22] or its earlier version. The authors in Refs. [20,21] discussed how much of the deformation parameter is reasonable to explain the observation, and pointed out the shortcoming of the QRPA in which the deformation parameters for the mother and daughter nuclei are the same.

Xu *et al.* carried out a systematic measurement of the β-decay $T_{1/2}$ of 20 neutron-rich nuclei in the ^{78}Ni region at the RIKEN-RIBF [16]. They found a sudden shortening of $T_{1/2}$ in the Ni isotopes beyond $N = 50$. When the β-decay Q_β value is sufficiently high, $T_{1/2}$ is well approximated by a fifth-power dependence on Q_β. Experimentally, the monotonic shortening of $\log_{10} T_{1/2}$ of the Ni isotopes as a function of the neutron number was observed below $N = 50$, indicating that the Q_β value gradually increases in the isotopic chain below ^{78}Ni. It was argued that the sudden shortening of $T_{1/2}$ beyond $N = 50$ is due to the sudden increase in Q_β because the nuclear deformation is not expected to occur: A large shell gap at $N = 50$ gives us a dramatic increase in Q_β. As mentioned in Ref. [16], the neutrons outside the $N = 50$ gap may have a contribution to the β-decay via the forbidden transitions. However, Borzov predicted that the first-forbidden (FF) transitions play only a minor role in the half-life of ^{79,80}Ni, while it is important for describing the β-decay properties around $N \simeq 82$ and 126, and the β-delayed neutron emission probability around ^{78}Ni [23,24]. Therefore, not only the shell gap, but also the details of the nuclear wave functions are needed to investigate for understanding the origin of the observed sudden shortening of $T_{1/2}$ in the Ni isotopes.

In the present article, I study systematically the β-decay $T_{1/2}$ in the neutron-rich Ni isotopes around ^{78}Ni. Then, I try to understand the microscopic mechanism for the observed sudden shortening of the half-lives. To this end, the β-strength distributions in the neutron-rich nuclei are described in a microscopic framework of nuclear density functional theory. Here, not only the allowed but the FF transitions are considered on the same footing.

This article is organized in the following way: The theoretical frameworks for describing the ground state and the nuclear matrix elements needed for the β-decay rates are given in Sec. II. Details of the numerical calculation are also given. However, part of the details on the matrix elements needed for the FF transitions are given separately in the Appendix. Section III is devoted to the numerical results and discussion based on the microscopic calculation. Then, a summary is given in Sec. IV.

II. THEORETICAL FRAMEWORK

A. HFB and pnQRPA for the nuclear matrix elements

In a framework of the nuclear energy-density functional (EDF) method I employed, the ground state of mother (target) nucleus is described by solving the Hartree-Fock-Bogoliubov (HFB) equation [25,26]

$$\begin{pmatrix} h^q(\boldsymbol{r}\sigma) - \lambda^q & \tilde{h}^q(\boldsymbol{r}\sigma) \\ \tilde{h}^q(\boldsymbol{r}\sigma) & -(h^q(\boldsymbol{r}\sigma) - \lambda^q) \end{pmatrix} \begin{pmatrix} \varphi^q_{1,\alpha}(\boldsymbol{r}\sigma) \\ \varphi^q_{2,\alpha}(\boldsymbol{r}\sigma) \end{pmatrix} = E_\alpha \begin{pmatrix} \varphi^q_{1,\alpha}(\boldsymbol{r}\sigma) \\ \varphi^q_{2,\alpha}(\boldsymbol{r}\sigma) \end{pmatrix}, \tag{1}$$

where the mean field and the pair field are given by the functional derivative of the EDF with respect to the density and the pair density, respectively. The superscript q denotes ν (neutron, $t_z = 1/2$) or π (proton, $t_z = -1/2$).

The excited states $|i\rangle$ of the daughter nucleus are described as a one-phonon excitation built on the ground state $|0\rangle$ of the mother (target) nucleus

$$|i\rangle = \hat{\Gamma}_i^\dagger |0\rangle, \tag{2}$$

$$\hat{\Gamma}_i^\dagger = \sum_{\alpha\beta} \left\{ X^i_{\alpha\beta} \hat{a}^\dagger_{\alpha,\nu} \hat{a}^\dagger_{\beta,\pi} - Y^i_{\alpha\beta} \hat{a}_{\bar{\beta},\pi} \hat{a}_{\bar{\alpha},\nu} \right\}, \tag{3}$$

where $\hat{a}^\dagger_\nu(\hat{a}^\dagger_\pi)$ and $\hat{a}_\nu(\hat{a}_\pi)$ are the neutron (proton) quasiparticle creation and annihilation operators. The phonon states, the amplitudes X^i, Y^i, and the vibrational frequency ω_i are obtained in the proton-neutron QRPA (pnQRPA).

The local one-body operators for the nuclear matrix elements relevant to the β-decay rates of the axial-vector and vector-type transitions are written by

$$^A\hat{O}_\pm = \frac{1}{2} \sum_{\sigma,\sigma'} \sum_{\tau,\tau'} \int d\boldsymbol{r} \langle\sigma|^A O(\boldsymbol{r},\boldsymbol{\sigma})|\sigma'\rangle \langle\tau|\tau_\pm|\tau'\rangle \times \hat{\psi}^\dagger(\boldsymbol{r}\sigma\tau)\hat{\psi}(\boldsymbol{r}\sigma'\tau'), \tag{4}$$

$$^V\hat{O}_\pm = \frac{1}{2} \sum_{\sigma,\sigma'} \sum_{\tau,\tau'} \int d\boldsymbol{r}\, ^V O(\boldsymbol{r}) \delta_{\sigma\sigma'} \langle\tau|\tau_\pm|\tau'\rangle \hat{\psi}^\dagger(\boldsymbol{r}\sigma\tau)\hat{\psi}(\boldsymbol{r}\sigma'\tau'), \tag{5}$$

TABLE I. Summary of ${}^{A}O(\boldsymbol{r},\boldsymbol{\sigma})[{}^{V}O(\boldsymbol{r})]$ in the operators ${}^{A(V)}\hat{O}^{JLK}$ needed for the matrix elements of the FF transitions, where $m_{\rm n}$ is the mass of the nucleon. The factor Θ_K arises from the transformation from the intrinsic to the laboratory frames of reference [27]: $\Theta_K = 1$ and $\sqrt{2}$ for $K = 0$ and $K \neq 0$, respectively.

${}^{A}\hat{O}^{000}$	${}^{A}\hat{O}^{J1K}$	${}^{V}\hat{O}^{10K}$	${}^{V}\hat{O}^{11K}$
$\frac{\boldsymbol{\sigma}\cdot\nabla}{m_{\rm n}}$	$\sqrt{\frac{4\pi}{3}}r[Y_1\otimes\boldsymbol{\sigma}]^J_K\Theta_K$	$\frac{\nabla_K}{m_{\rm n}}\Theta_K$	$\sqrt{\frac{4\pi}{3}}rY_{1K}\Theta_K$

respectively, where $\boldsymbol{\sigma} = (\sigma_{-1}, \sigma_0, \sigma_{+1})$ denotes the spherical components of the Pauli spin matrices, and $\tau_\pm = (\tau_x \pm i\tau_y)$ are the isospin-ladder operators. The nucleon field operators $\hat{\psi}^\dagger$ and $\hat{\psi}$ are expressed in terms of the quasiparticle operators $\hat{a}^\dagger$ and $\hat{a}$ through the generalized Bogoliubov transformation. I consider the allowed and FF transitions in the present calculation. For the allowed transitions, the operators needed are just for ${}^{A}O(\boldsymbol{r},\boldsymbol{\sigma}) = \boldsymbol{\sigma}$ and ${}^{V}O(\boldsymbol{r}) = 1$, while for the FF transitions, one needs the operators for those containing rY_1 and those appearing due to the relativistic correction as summarized in Table I. Here, the operators ${}^{A}\hat{O}^{J1K}$ and ${}^{V}\hat{O}^{11K}$ correspond to the charge-exchange rank-J spin-dipole and dipole operators, respectively. The nuclear transition matrix elements $\langle i|\hat{O}|0\rangle$ are evaluated in the standard quasi-boson approximation as $\langle \mathrm{HFB}|[\hat{\Gamma}_i, \hat{O}]|\mathrm{HFB}\rangle$.

B. Numerical calculations

I solved the coordinate-space HFB equations in the cylindrical coordinates $\boldsymbol{r} = (\rho, z, \phi)$ with a mesh size of $\Delta\rho = \Delta z = 0.6$ fm and a box boundary condition at $(\rho_{\max}, z_{\max}) = (14.7, 14.4)$ fm. The qp states were truncated according to the qp energy cutoff at 60 MeV, and the qp states up to the magnetic quantum number $\Omega = 23/2$ with positive and negative parities were included.

The two-body interactions for the pnQRPA equation were derived self-consistently from the EDF. I introduced the truncation for the two-quasiparticle (2qp) configurations in the QRPA calculation, in terms of the 2qp-energy as 60 MeV. More details of the calculation scheme are given in Ref. [28].

For the normal (particle-hole) part of the EDF, I employed mainly the SkM* functional [29] and secondarily the SLy4 functional [30]. For the pairing energy, I adopted the one in Ref. [31] that depends on both the isoscalar and isovector densities, in addition to the pairing density, with the parameters given in Table III of Ref. [31]. The same pairing EDF was employed for the $T = 1$ pn-pairing interaction in the pnQRPA calculation, while the linear term in the isovector density was dropped. The $T = 0$ pairing interaction was also included in the present pnQRPA calculation, with the same strength as the $T = 1$ pairing interaction. Though I did not optimize the pairing strengths, the characteristic isotopic dependence was reproduced well by the present work.

C. Calculation of the β-decay rates

The β-decay rate λ_β and the partial half-life $t_{1/2}$ including the allowed and FF transitions can be calculated as [32,33]

$$\frac{1}{t_{1/2}} = \frac{\lambda_\beta}{\ln 2} = \frac{f}{D}, \tag{6}$$

$$f = \int_1^{W_0} C(W)F(Z,W)pW(W_0 - W)^2 dW, \tag{7}$$

where I used $D = 6147$ s for the constant, and $C(W)$ is the shape factor containing the nuclear matrix elements as described below. The Fermi function $F(Z, W)$ in Eq. (7) including the effect of the Coulomb distortion on the electron wave function is given by

$$F(Z,W) = 2(1+\gamma)(2pR)^{-2(1-\gamma)}e^{\pi\nu}\left|\frac{\Gamma(\gamma+i\nu)}{\Gamma(2\gamma+1)}\right|^2, \tag{8}$$

where $\gamma = \sqrt{1-(\alpha Z)^2}$, $\nu = \alpha ZW/p$, α is the fine-structure constant, and R is the nuclear radius calculated as $1.2 \times A^{1/3}$ fm. W is the total energy of the electron, W_0 is the total energy available;

$$W_0 = m_e c^2 + \lambda_\nu - \lambda_\pi + \Delta M_{n-H} - \omega_i \tag{9}$$

$$= m_e c^2 - E_{{\rm T},i} + \Delta M_{n-H}, \tag{10}$$

and $p = \sqrt{W^2 - 1}$ is the momentum. $\Delta M_{n-H} = 0.782$ MeV is a mass difference between a neutron and a hydrogen atom, and $E_{{\rm T},i}$ the excitation energy with respect to the ground state of the mother (target) nucleus, and $\lambda_{\pi(\nu)}$ the chemical potential of protons (neutrons). In the followings, I use natural units $\hbar = c = m_e = 1$. The unit of length is the reduced electron Compton wavelength $\lambda\!\!\!^{-}_e = 386.16$ fm.

The shape factor for the allowed transitions is given as

$$C_0 = |\langle 1\rangle|^2 + \lambda^2|\langle\boldsymbol{\sigma}\rangle|^2, \tag{11}$$

where $\langle\cdot\rangle$ denotes the nuclear transition matrix element between the ground and excited states $|i\rangle$ for the isospin lowering operator, and $\lambda = -(g_A/g_V) = 1.2701(25)$ is the ratio of weak axial and vector coupling constants. I used the quenching factor for the allowed Gamow-Teller transitions as $q = g_A^{\rm eff}/g_A = 0.79$ or equivalently $\lambda^{\rm eff} = 1$, as commonly used in the pnQRPA framework [22,34–37]. Since the shape factor C_0 is independent of the energy W, it is convenient to define the phase-space factor, or the so-called integrated Fermi function f_0 as

$$ft_{1/2} = C_0 f_0 t_{1/2} = D, \tag{12}$$

$$f_0 = \int_1^{W_0} F(Z,W)pW(W_0 - W)^2 dW. \tag{13}$$

When the FF transitions take part in the β-decay process, one needs to consider the explicit dependence of the shape factors on the electron energy as the details are given in the Appendix. To discuss the FF transition strengths distribution and compare to the allowed transitions relevant to the β-decay, it is useful to define the averaged shape factor as [32]

$$\overline{C(W)} = \frac{f}{f_0}, \tag{14}$$

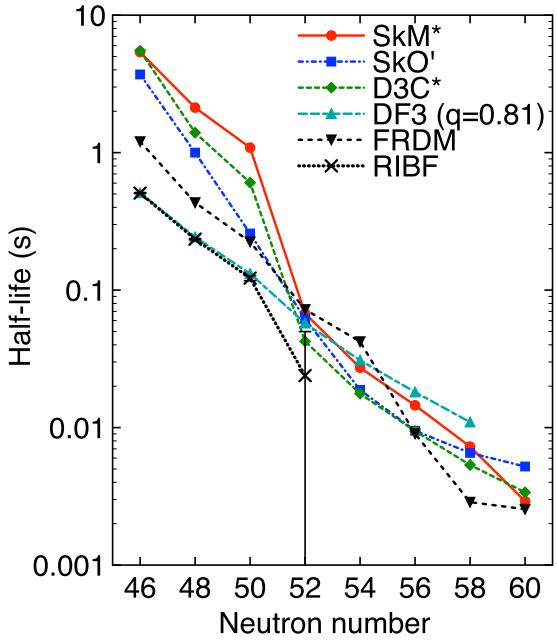

FIG. 1. Calculated β-decay half-lives of the neutron-rich Ni isotopes with use of the SkM* functional. Shown together with the results in the preceding pnQRPA calculations [22,24,35,36] and the half-lives measured at the RIKEN-RIBF [16].

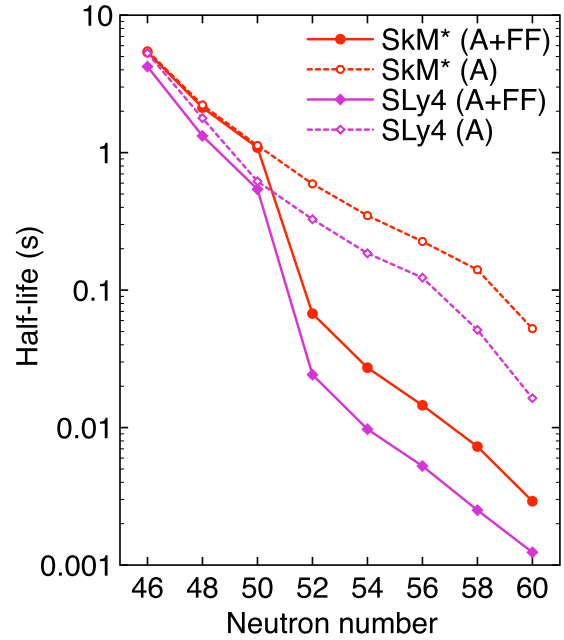

FIG. 2. Similar to Fig. 1 but employing the SLy4 functional besides the SkM* functional. Shown are also the results obtained in the allowed approximation denoted by the open symbols.

so that the partial half-life is related to $\overline{C(W)}$ as $D/f_0 t_{1/2}$ similarly to the allowed transitions. The total half-life $T_{1/2}$ is calculated by summing all the energetically possible transitions; $W_0 > 1$.

III. RESULTS AND DISCUSSION

Figure 1 shows the calculated β-decay half-lives of the neutron-rich even-N Ni isotopes by using the SkM* functional. A sudden shortening of the half-lives beyond $N = 50$ is clearly seen. Up to $N = 50$ and above $N = 52$, the calculation shows a monotonic decrease in the half-lives. One can thus expect something singular to have happened between $N = 50$ and 52. In what follows, I am going to discuss the mechanism for this sudden shortening of the half-lives beyond $N = 50$. It is noted that the Ni isotopes under investigation are all calculated to be spherical in the present framework. So the acceleration is not due to the nuclear shape effect.

Before discussing the isotopic dependence of the calculated half-lives, I briefly mention the results obtained in the preceding pnQRPA calculations, which are also shown in Fig. 1. The calculation employing the relativistic functional D3C* [36] gives the similar result to that using the SkM* functional, while the other microscopic calculations shown here [24,35] produce the monotonic decrease. Taking a closer look at the result of the FRDM [22], where the FF transitions are taken into account by the gross theory, one sees that the model predicts a sudden shortening beyond $N = 54$ although the previous version of the model based on the allowed approximation already predicted this behavior [38]. The calculations except that using DF3 [24], where the large quenching factor $q^2 = 0.81$ was used, i.e., less quenching of g_A, overestimate the observed half-lives. Though it is beyond the scope of the present work, there is room for further investigation on the roles of 2p2h configurations, namely the beyond-RPA effects such as in a particle-vibration coupling scheme as discussed in Ref. [39].

I show in Fig. 2 the calculated β-decay half-lives obtained in the allowed (A) approximation and those where the FF transitions are also taken into account (A + FF). The calculations in the A approximation only produce the monotonic shortening, while those in the A + FF approximation give a sudden shortening at $N = 52$. Not only the calculation using SkM* but that using the SLy4 functional produce the sudden shortening. Thus, the FF transitions are necessary to explain the observed sudden shortening of the β-decay half-lives. The calculation scheme in Ref. [35] is analogous to the present one in the sense that the Skyrme-type EDF was employed for the HFB + pnQRPA calculation and the FF transitions were taken into account in a microscopic way. The only difference to the present calculation is that the SkO′ functional [40] was used there. I am going to investigate the reason why the SkM*, SLy4, and D3C* functionals produce the sudden shortening, while SkO′ only produces the monotonic one for the β-decay half-lives, then unravel the mechanism for the sudden shortening beyond $N = 50$.

Figure 3 displays the FF contribution to the computed total β-decay rate. The calculations using the SkM*, SLy4, and D3C* functionals show that the FF transitions largely contribute to the β-decay rate at $N = 52$ while the FF contribution is low at $N = 50$. However, the calculation using SkO′ only shows the monotonic increase in the FF contribution as the neutron number increases from 46 to 52, and the much less FF contribution than the others for $N \geqslant 54$. The similar feature can be also seen in the calculation employing DF3. Therefore,

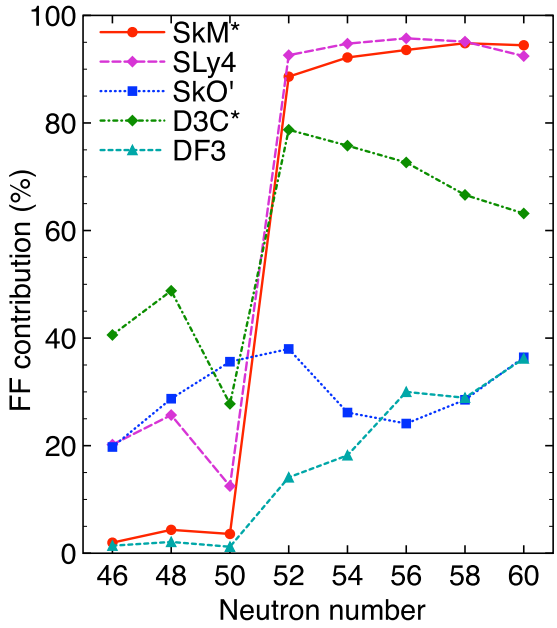

FIG. 3. FF contribution to the total β-decay rate computed using the Skyrme-type EDFs of SkM* and SLy4 in the present calculation, and SkO′ in Ref. [35], the relativistic EDF of D3C* in Ref. [36], and DF3 in Ref. [41].

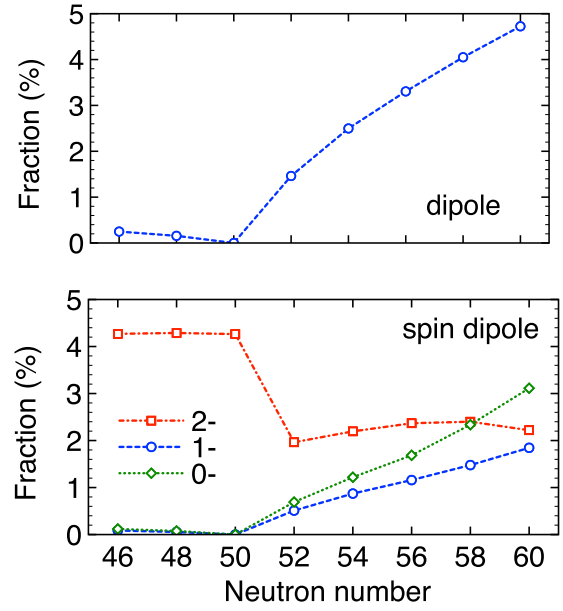

FIG. 4. Fraction of the summed strengths of the dipole (top) and the spin dipole (bottom) transitions in low energy below $E_{\rm T} < 0$ calculated using the SkM* functional.

the onset of the FF transitions beyond $N = 50$ is a key to the understanding of the mechanism for the sudden shortening of the β-decay half-lives in the neutron-rich Ni isotopes.

The onset of the FF transitions beyond $N = 50$ is simply understood by the appearance of the low-energy $-1\hbar\omega_0$ excitation associated with the shell structure in neutron-rich nuclei [42]. In the light nuclei around $A \simeq 40$, the similar mechanism for the onset of the FF transitions beyond $N = 28$ was also discussed [43]. Figure 4 shows the fraction of the summed strengths of the dipole ($\Delta J^\pi = 1^-$) and the spin dipole ($\Delta J^\pi = 0^-, 1^-$, and 2^-) transitions in low energy below $E_{\rm T} < 0$. The upper figure in Fig. 4 corresponds to Fig. 3(b) in Ref. [42]. As the neutrons start to occupy the $2d_{5/2}$ and $2d_{3/2}$ orbitals, the negative-parity $\nu d_{5/2}, d_{3/2} \to \pi p_{3/2}, p_{1/2}$ excitations are possible to occur. From this figure, one sees that the 0^- and 1^- excitations are crucial for the acceleration in $T_{1/2}$ between $N = 50$ and 52. The contribution of the 2^- excitation is anticorrelated with the decrease in $T_{1/2}$. Figure 5 displays the shape factors and the averaged shape factors for the allowed and the FF transitions from ^{76,82}Ni. As can be seen in Fig. 5(b), several negative-parity states possessing an appreciable strength show up.

I am going to discuss further the microscopic origin of the sudden onset of the FF transitions beyond $N = 50$. I show in Fig. 6 the contribution of the FF multipoles to the total β-decay rate obtained by using SkM*. One clearly sees that the 0^- and 1^- transitions are dominant beyond $N = 50$. This can be understood by the location of the Fermi level of neutrons. Up to $N = 50$, the $g_{9/2}$ orbital is the only positive-parity occupied level. So the $\nu g_{9/2} \to \pi f_{5/2}$ FF transition with $\Delta J^\pi = 2^-$ is the only possible outcome. When the Fermi level moves to the $d_{5/2}$ orbital, the partially occupied neutrons in the $d_{5/2}$ orbital can participate in the $\nu d_{5/2} \to \pi f_{5/2}$ excitation with $\Delta J^\pi = 0^-$ and the $\nu d_{5/2} \to \pi p_{3/2}$ excitation with $\Delta J^\pi = 1^-$ besides the $\nu d_{5/2} \to \pi p_{1/2}$ excitation with $\Delta J^\pi = 2^-$ transition. One sees these excitations in the averaged shape factors for the FF transitions displayed in Fig. 5(b). The low-lying prominent peaks in ^{80,82}Ni correspond to the $\Delta J^\pi = 0^-$ and 1^- excitations. Furthermore, in the relatively higher energy region $E_{\rm T} \sim -5$ MeV, one sees the $\nu g_{9/2} \to \pi f_{5/2}$ excitation.

One more important thing for the sudden onset of the FF transitions beyond $N = 50$ is the magnitude of the relative energy between the FF and allowed transitions. One sees in Fig. 5(a) a prominent peak in the shape factor around $E_{\rm T} \sim -5$ MeV, which is above the FF transition by about 5 MeV. This is predominantly constructed by the $\nu p_{1/2} \to \pi p_{3/2}$ excitation with the RPA amplitude $X^2 - Y^2$ being greater than 0.9. The transition strength for this allowed transition is much larger than that for the FF transitions. Since the phase-space factor f_0 roughly behaves as W_0^5, the FF transitions are able to overcome the contribution from the allowed transitions if they are high enough in energy, and are well apart from the allowed transitions. In the present case, the FF transitions gain a factor $\sim(10/5)^5 = 32$ from the phase space factor. Therefore, the contribution from the FF transitions at $N = 52$ dominates that from the allowed transitions.

The appearance of the high-energy FF transitions is a key mechanism for the characteristic isotopic dependence of the half-lives. However, the β-strength function is hard to observe experimentally. The β-delayed neutron emission probability P_n combined with $T_{1/2}$ may access the distribution indirectly because the transitions lower than $Q_\beta - S_n$ in energy contribute to the neutron emission while the transitions up to Q_β to the half-life, here Q_β and S_n are the ground-state β-decay Q-value and the neutron separation energy of the daughter nucleus. If there is an appreciable strength in high energy (in

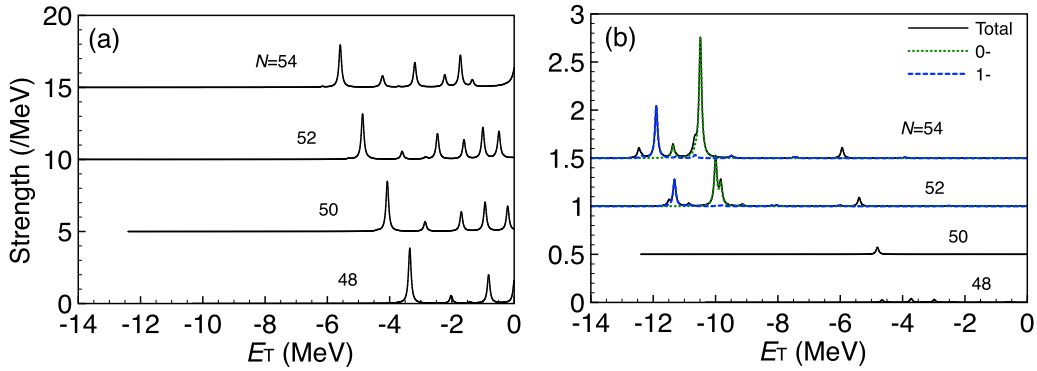

FIG. 5. Shape factors and the averaged shape factors for (a) the allowed and (b) the FF transitions from $^{76-82}$Ni calculated by using the SkM* functional.

the low-lying region of the daughter), the P_n value is hindered while $T_{1/2}$ is short as discussed in Refs. [24,43].

The low-lying states relevant to the β-decay rate are weakly collective in the present calculation for the Ni isotopes. Thus, I can discuss qualitatively the competitive roles played by the allowed and FF transitions in terms of the single-particle levels around the Fermi levels. I show in Fig. 7 the single-particle energies of neutrons and protons relative to that of the $\nu 2p_{1/2}$ and $\pi 1f_{7/2}$ orbitals, respectively, calculated using the SkM*, SLy4, SkO′, and D3C* functionals. As discussed above, the $\nu g_{9/2} \to \pi f_{5/2}$ excitation is only available up to $N = 50$ for the FF transition, and the $\nu p_{1/2} \to \pi p_{3/2}$ excitation dominantly contributes to the allowed transitions. So the size of $N = 40$ gap and the relative location between the $\pi f_{5/2}$ and $\pi p_{3/2}$ levels govern the β-decay rate for $N \leqslant 50$. As the shell gap at $N = 40$ is small, the energy difference between the allowed and FF transitions is small. Thus, the FF contribution is small. In the calculation using SkM* since the $\pi f_{5/2}$ level is located above the $\pi p_{3/2}$ level by 1.5 MeV, the FF contribution is strongly suppressed. On the other hand, as seen in the calculations with the SLy4, D3C*, and SkO′ functionals, the FF contribution is larger as the $N = 40$ gap increases.

Beyond $N = 50$, the multiple FF transitions involving the $\nu 2d_{5/2}$ orbital are possible to occur. The larger the sum of the gap energy of the $N = 40$ and 50, the larger the FF contribution is. This is because the energy difference between the allowed and FF excitations is large. For a sudden onset of the FF contribution above $N = 50$, preferable is the situation in which an $N = 50$ gap is large and an $N = 40$ gap is instead small.

Since the sudden shortening of the half-lives beyond $N = 50$ was observed only in the Ni isotopes, this is considered as evidence of the proton shell closure at $Z = 28$ as well as the neutron shell closure at $N = 50$, namely this is due to that ^{78}Ni is a doubly magic nucleus [16]. Before summarizing this article let me discuss what is happening in the Zn ($Z = 30$) isotopes.

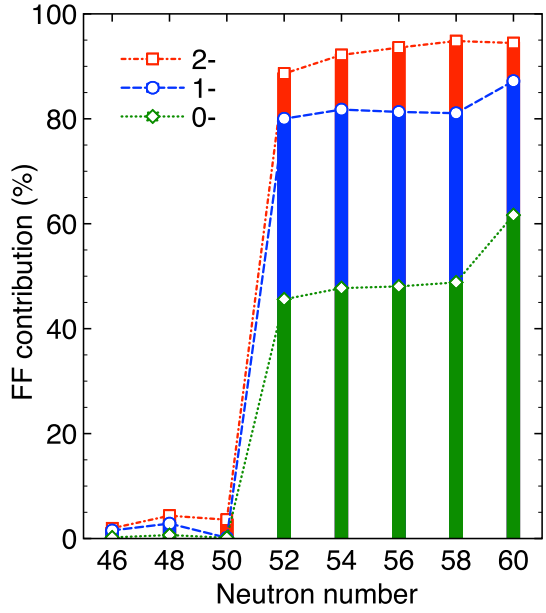

FIG. 6. Contributions of the different FF multipoles to the total β-decay rate computed by using the SkM* functional.

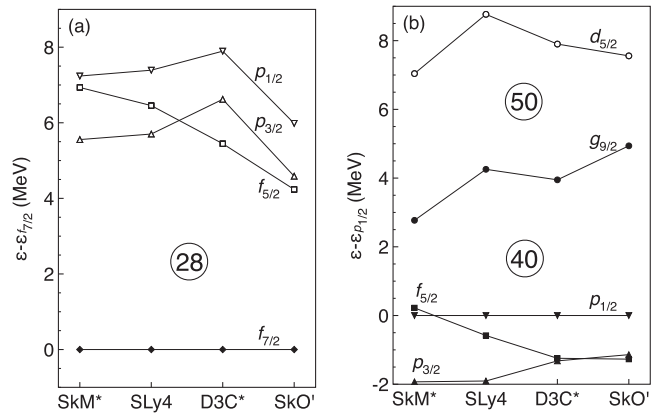

FIG. 7. (a) Proton's single-particle energies relative to that of the $1f_{7/2}$ orbital, and (b) neutron's ones relative to that of the $2p_{1/2}$ orbital calculated by using several EDFs in ^{78}Ni. The result for D3C* was obtained in Refs. [36,44], and that for SkO′ was obtained by using HFBRAD [45]. The filled and open symbols indicate the occupied and unoccupied levels, respectively.

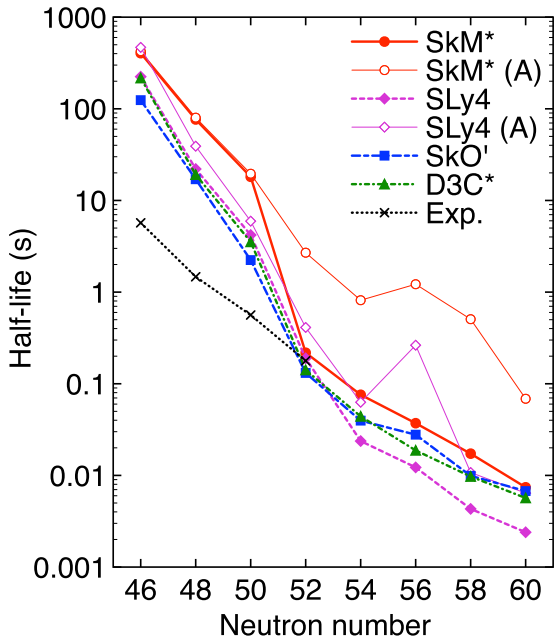

FIG. 8. Similar to Fig. 1 except for the Zn isotopes. The results obtained in the allowed approximation are also shown for the calculations using the SkM* and SLy4 functionals.

Figure 8 shows the calculated β-decay half-lives of the Zn isotopes around $N = 50$. As in the case for the Ni isotopes, the microscopic EDF calculations overestimate the observed half-lives for the low-N isotopes. However, one sees that the calculations except using the SkM* functional give a monotonic shortening of the half-lives up to $N = 54$ (SLy4) and $N = 52$ (SkO′ and D3C*). Beyond this, the half-lives decrease gently. Thus no abrupt change is seen in the Zn isotopes.

The results obtained in the allowed approximation are also shown for the calculations using the SkM* and SLy4 functionals in Fig. 8. The SkM* gives an onset of the FF transitions beyond $N = 50$ as in the Ni isotopes, while the SLy4 predicts that the FF transitions contribute to the β-decay almost constantly. This difference can be seen in the strengths distribution. Shown in Fig. 9 are the shape factors and the averaged shape factors for the allowed and the FF transitions from $^{78-84}$Zn. Let me discuss the case for SLy4. Below $N = 50$, the transition of the $\nu g_{9/2} \rightarrow \pi f_{5/2}$ excitation is located lower than SkM* thus giving a larger FF contribution. Beyond $N = 50$, there show up some tiny strengths for the high-energy allowed transition, which suppresses the FF contribution. A difference in between the Ni and Zn isotopes is that the Zn isotopes are deformed, and the magnitude of deformation is different depending on the functional employed: The deformation parameters calculated with SkM* (SLy4) are 0.08 (0.15) and 0.11 (0.16) for $N = 52$ and 54, respectively. A strange behavior seen around $N = 56$ is due to the subshell closure.

IV. SUMMARY

I carried out a systematic calculation of the β-decay rates for the neutron-rich Ni isotopes around $N = 50$ by means of the fully self-consistent proton-neutron-QRPA with the Skyrme EDFs. The experimentally observed sudden shortening of the half-lives beyond $N = 50$ was reproduced well by the calculations employing the Skyrme SkM* and SLy4 functionals. I found that the onset of the first-forbidden (FF) transitions plays a decisive role for the sudden shortening of the half-life in ^{80}Ni. This is due to a small subshell gap at $N = 40$ and a large shell gap at $N = 50$; the former suppresses the contribution from the FF transitions below $N = 50$ and the latter enhances it above $N = 50$. The present study reveals that a microscopic calculation taking the shell structure in neutron-rich nuclei and its associated effects on the FF transitions into account is necessary for predicting the β-decay rates of nuclei far from stability.

ACKNOWLEDGMENTS

The author thanks J. Engel and T. Marketin for valuable communications, and N. Van Giai for discussions. This work was supported by the JSPS KAKENHI (Grants No. JP16K17687, No. JP18H04569, No. JP19K03824, and No. JP19K03872), and the JSPS-NSFC Bilateral Program for Joint Research Project on "Nuclear mass and life for unraveling mysteries of the r-process." The numerical calculations were performed on CRAY XC40 at the Yukawa Institute for Theoretical Physics, Kyoto University, and on COMA (PACS-IX) at the Center for Computational Sciences, University of Tsukuba.

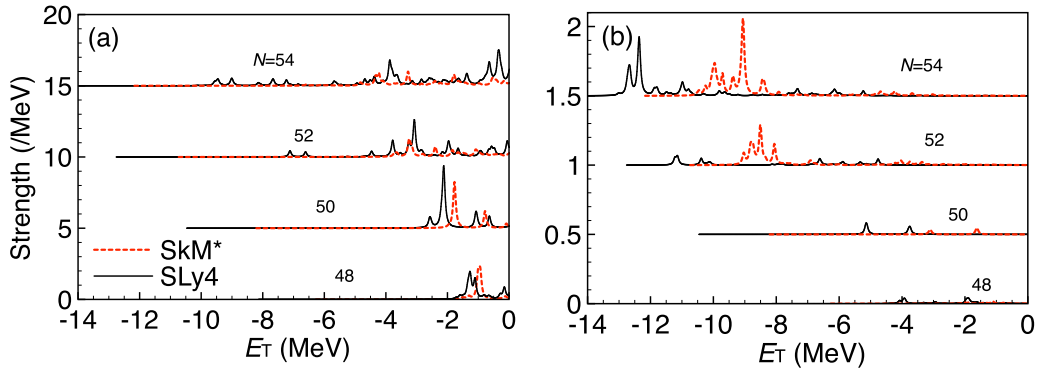

FIG. 9. Similar to Fig. 5 but for $^{78-84}$Zn obtained by using the SkM* and SLy4 functionals.

APPENDIX: FIRST-FORBIDDEN β-DECAY RATES

1. Shape factors

The shape factor for the FF transitions is energy dependent and given as [33]

$$C(W) = k + kaW + kb/W + kcW^2, \tag{A1}$$

where the coefficients k, ka, kb, and kc depend on the nuclear matrix elements and the maximum electron energy W_0. The nonvanishing coefficients are

$$\begin{aligned} k &= \zeta_0^2 + \tfrac{1}{9}w^2, \\ kb &= -\tfrac{2}{3}\mu_1\gamma_1\zeta_0 W, \end{aligned} \tag{A2}$$

for rank 0,

$$\begin{aligned} k =& \zeta_1^2 + \tfrac{1}{9}(x+u)^2 - \tfrac{4}{9}\mu_1\gamma_1 u(x+u) \\ &+ \tfrac{1}{18}W_0^2(2x+u)^2 - \tfrac{1}{18}\lambda_2(2x-u)^2, \\ ka =& -\tfrac{4}{3}uY - \tfrac{1}{9}W_0(4x^2+5u^2), \\ kb =& \tfrac{2}{3}\mu_1\gamma_1\zeta_1(x+u), \\ kc =& \tfrac{1}{18}[8u^2 + (2x+u)^2 + \lambda_2(2x-u)^2], \end{aligned} \tag{A3}$$

for rank 1, and

$$\begin{aligned} k &= \tfrac{1}{12}z^2(W_0 - \lambda_2), \\ ka &= -\tfrac{1}{6}z^2 W_0, \\ kc &= \tfrac{1}{12}z^2(1+\lambda_2), \end{aligned} \tag{A4}$$

for rank 2, respectively, with V, Y, ζ_0, and ζ_1 being defined by

$$\begin{aligned} V &= \xi' v + \xi w', \\ \zeta_0 &= V + \tfrac{1}{3}wW_0, \\ Y &= \xi' y - \xi(u' + x'), \\ \zeta_1 &= Y + \tfrac{1}{3}(u-x)W_0. \end{aligned} \tag{A5}$$

$$\tag{A6}$$

Here the dimensionless parameter ξ is defined as $\xi = \alpha Z/2R$. The Coulomb functions μ_1 and λ_2 are defined in terms of electron wave functions and depend on the electron momentum [33]. These values are close to unity, so I use the approximations $\mu_1 = 1$ and $\lambda_2 = 1$ as usually adopted [46].

The matrix elements are related to the form factors ${}^{A(V)}F_{Jls}$ as [32]

$$w = -R\,{}^{A}F_{011} = \sqrt{3}\lambda\langle {}^{A}\hat{O}_{-}^{01K}\rangle, \tag{A7a}$$

$$x = -\frac{1}{\sqrt{3}}R\,{}^{V}F_{110} = -\langle {}^{V}\hat{O}_{-}^{11K}\rangle, \tag{A7b}$$

$$u = -\sqrt{\frac{2}{3}}R\,{}^{A}F_{111} = \sqrt{2}\lambda\langle {}^{A}\hat{O}_{-}^{11K}\rangle, \tag{A7c}$$

$$z = \frac{2}{\sqrt{3}}R\,{}^{A}F_{211} = -2\lambda\langle {}^{A}\hat{O}_{-}^{21K}\rangle, \tag{A7d}$$

$$\xi' v = {}^{A}F_{000} = -\sqrt{3}\lambda\langle {}^{A}\hat{O}_{-}^{000}\rangle, \tag{A7e}$$

$$\xi' y = {}^{V}F_{101} = -\langle {}^{V}\hat{O}_{-}^{10K}\rangle, \tag{A7f}$$

where $\lambda = -(g_A/g_V) = 1.27$. For the FF transitions, no quenching factors are introduced for simplicity in the present calculation as in Ref. [35]. The primed matrix elements w', x', and u' are calculated with the operator multiplied by

$$\begin{cases} 1 - \dfrac{1}{5}\left(\dfrac{r}{R}\right)^2, & 0 < r < R, \\ \dfrac{R}{r} - \dfrac{1}{5}\left(\dfrac{r}{R}\right)^3, & r > R, \end{cases} \tag{A8}$$

where $r = \sqrt{\rho^2 + z^2}$ in the cylindrical coordinates.

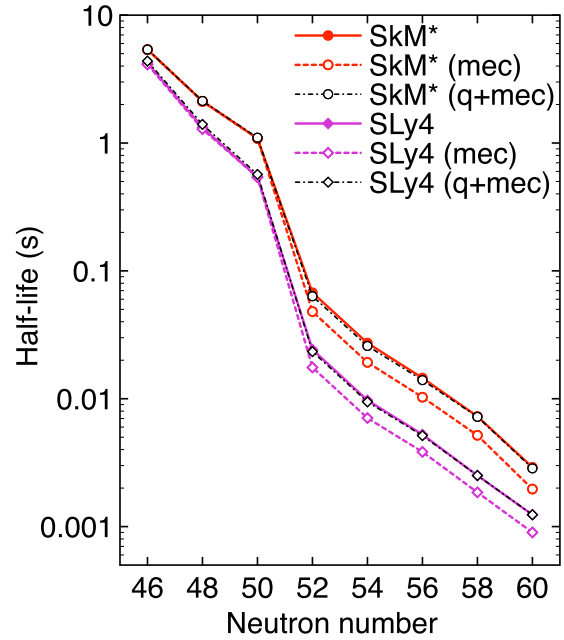

FIG. 10. Similar to Fig. 2 but the mesonic enhancement and the quenching effects are included. A scaling factor 1.5 is multiplied for the matrix element $\xi' v$ (mec). Further, the same quenching factor $q = 0.79$ is used for the FF transition as for the allowed transition (q + mec).

2. Effects of the (anti)quenching of the FF transitions

Since the present article discusses an important role of the nonunique FF transitions for a sudden shortening of the β-decay half-lives in the Ni isotopes above $N = 50$, it should be noted that an enhancement effect of the rank-zero FF transition due to the meson exchange current [46–48] occurs. To consider this effect in a practical calculation, a scaling factor is introduced for the matrix element $\xi' v$ of Eq. (A7e) as an effective operator [46].

Figure 10 shows the computed β-decay half-lives by using the SkM* and SLy4 functionals including the scaling factor. One sees that the enhancement in the matrix element leads to a further shortening of the half-lives irrespective of the EDF employed. The mesonic enhancement in the FF transition fortifies the mechanism for the sudden shortening of the β-decay half-lives beyond the $N = 50$ magic number.

The quenching for the FF transitions is also discussed [49], and one needs to consider not only the enhancement but the quenching simultaneously. Here the same quenching factor is employed for the FF transitions as used for the allowed

transition: $g_A^{\text{eff}} = q \times g_A$. It is found that the calculated β-decay half-lives come closer to the results obtained in the simple prescription where the quenching is considered only for the allowed transitions. Therefore, the discussions made in the present article are robust against the details of the enhancement and quenching of the FF transitions.

[1] O. Sorlin and M.-G. Porquet, Prog. Part. Nucl. Phys. **61**, 602 (2008).
[2] T. Otsuka, A. Gade, O. Sorlin, T. Suzuki, and Y. Utsuno, arXiv:1805.06501.
[3] P. T. Hosmer *et al.*, Phys. Rev. Lett. **94**, 112501 (2005).
[4] J. Hakala *et al.*, Phys. Rev. Lett. **101**, 052502 (2008).
[5] A. Welker *et al.*, Phys. Rev. Lett. **119**, 192502 (2017).
[6] S. Baruah *et al.*, Phys. Rev. Lett. **101**, 262501 (2008).
[7] M.-G. Porquet and O. Sorlin, Phys. Rev. C **85**, 014307 (2012).
[8] Y. H. Zhang *et al.*, Phys. Rev. C **70**, 024301 (2004).
[9] E. Padilla-Rodal *et al.*, Phys. Rev. Lett. **94**, 122501 (2005).
[10] M. Lebois *et al.*, Phys. Rev. C **80**, 044308 (2009).
[11] A. Gade *et al.*, Phys. Rev. C **81**, 064326 (2010).
[12] J. Van de Walle, Phys. Rev. Lett. **99**, 142501 (2007).
[13] Y. Shiga, Phys. Rev. C **93**, 024320 (2016).
[14] N. Aoi *et al.*, Phys. Lett. B **692**, 302 (2010).
[15] R. Taniuchi *et al.*, Nature **569**, 53 (2019).
[16] Z. Y. Xu *et al.*, Phys. Rev. Lett. **113**, 032505 (2014).
[17] K. Sieja and F. Nowacki, Phys. Rev. C **85**, 051301(R) (2012).
[18] G. Hagen, G. R. Jansen, and T. Papenbrock, Phys. Rev. Lett. **117**, 172501 (2016).
[19] F. Nowacki, A. Poves, E. Caurier, and B. Bounthong, Phys. Rev. Lett. **117**, 272501 (2016).
[20] O. Sorlin *et al.*, Phys. Rev. C **47**, 2941 (1993).
[21] J. M. Daugas *et al.*, Phys. Rev. C **83**, 054312 (2011).
[22] P. Möller, B. Pfeiffer, and K. L. Kratz, Phys. Rev. C **67**, 055802 (2003).
[23] I. N. Borzov, Phys. Rev. C **67**, 025802 (2003)
[24] I. N. Borzov, Phys. Rev. C **71**, 065801 (2005).
[25] J. Dobaczewski, H. Flocard, and J. Treiner, Nucl. Phys. A **422**, 103 (1984).
[26] A. Bulgac, arXiv:nucl-th/9907088.
[27] A. Bohr and B. R. Mottelson, *Nuclear Structure* (Benjamin, New York, 1975), Vol. II.
[28] K. Yoshida, Prog. Theor. Exp. Phys. **2013**, 113D02 (2013).
[29] J. Bartel, P. Quentin, M. Brack, C. Guet, and H.-B. Håkansson, Nucl. Phys. A **386**, 79 (1982).
[30] E. Chabanat, P. Bonche, P. Haensel, J. Meyer, and R. Schaefer, Nucl. Phys. A **635**, 231 (1998); **643**, 441(E) (1998).
[31] M. Yamagami, Y. R. Shimizu, and T. Nakatsukasa, Phys. Rev. C **80**, 064301 (2009).
[32] H. Behrens and W. Bühring, *Electron Radial Wave Functions and Nuclear Beta-Decay* (Clarendon, Oxford, 1982).
[33] H. F. Schopper, *Weak Interactions and Nuclear Beta Decay* (North-Holland, Amsterdam, 1966).
[34] J. Engel, M. Bender, J. Dobaczewski, W. Nazarewicz, and R. Surman, Phys. Rev. C **60**, 014302 (1999).
[35] M. T. Mustonen and J. Engel, Phys. Rev. C **93**, 014304 (2016).
[36] T. Marketin, L. Huther, and G. Martínez-Pinedo, Phys. Rev. C **93**, 025805 (2016).
[37] P. Sarriguren, A. Algora, and G. Kiss, Phys. Rev. C **98**, 024311 (2018).
[38] P. Möller, J. R. Nix, and K.-L. Kratz, At. Data Nucl. Data Tables **66**, 131 (1997).
[39] Y. F. Niu, G. Colò, E. Vigezzi, C. L. Bai, and H. Sagawa, Phys. Rev. C **94**, 064328 (2016).
[40] P. G. Reinhard, D. J. Dean, W. Nazarewicz, J. Dobaczewski, J. A. Maruhn, and M. R. Strayer, Phys. Rev. C **60**, 014316 (1999).
[41] I. N. Borzov, and S. V. Tolokonnikov, in *Proceedings of IX International Symposium EXON-2018, 4-10 Sept., Petrozavodsk, Russia* (World Scientific, Singapore, 2017).
[42] K. Yoshida, Phys. Rev. C **96**, 051302(R) (2017).
[43] S. Yoshida, Y. Utsuno, N. Shimizu, and T. Otsuka, Phys. Rev. C **97**, 054321 (2018).
[44] T. Marketin (private communication).
[45] K. Bennaceur and J. Dobaczewski, Comput. Phys. Commun. **168**, 96 (2005).
[46] E. K. Warburton, J. A. Becker, B. A. Brown, and D. J. Millener, Ann. Phys. (NY) **187**, 471 (1988).
[47] E. K. Warburton, Phys. Rev. C **44**, 233 (1991).
[48] I. S. Towner, Nucl. Phys. A **542**, 631 (1992).
[49] J. T. Suhonen, Front. Phys. **5**, 55 (2017).